Materials Today Communications 23 (2020) 100917

Contents lists available at ScienceDirect

Materials Today Communications

journal homepage: www.elsevier.com/locate/mtcomm

Mechanical response of low density expanded polypropylene foams in compression and tension at different loading rates and temperatures

Daniel T. Morton[a,b,*], Aase Reyes[a,b,c], Arild H. Clausen[a,b], Odd Sture Hopperstad[a,b]

[a] Structural Impact Laboratory (SIMLab), Department of Structural Engineering, Norwegian University of Science and Technology (NTNU), NO-7491, Trondheim, Norway
[b] Centre for Advanced Structural Analysis (CASA), NTNU, NO-7491, Trondheim, Norway
[c] Department of Civil Engineering and Energy Technology, Oslo Metropolitan University, Post box 4, St. Olavs plass, NO-0130, Oslo, Norway

ARTICLE INFO

Keywords:
Cellular material
Material tests
Expanded polypropylene foam (EPP)
Temperature effect
Strain rate effect
Mechanical properties

ABSTRACT

Polymer foams are often used for impact mitigation and protection due to low weight and excellent energy absorbing capability. Depending on the application, different loading rates and environmental conditions can be expected, including various operating temperatures. In this paper, experimental results from mechanical testing of expanded polypropylene (EPP) are presented, focusing on temperature and rate dependence. The compressive and tensile responses of two EPP foams of similar nominal density (30 kg/m^3) but different morphology are compared. Both foams were tested in compression at low to intermediate strain rates (10^{-3} to 10^0s^{-1}) to determine the strain rate dependence. The temperature dependence of one foam type was quantified in both compression and tension for temperatures between − 30°C and 60°C in order to highlight the importance of operating temperature. It was found that both strain rate and temperature have a definitive effect on the mechanical properties. The morphology of the two EPP foams also seems to affect the response.

1. Introduction

Energy absorption and impact mitigation are typical applications where polymer foams are utilized. Examples include packaging, helmets and pedestrian impact protection [1,2]. Polymer foams can be tailored to specific applications by choosing an appropriate bulk material and manufacturing process. Desirable qualities include low density and good energy absorption capability. Foams are typically defined as cellular materials with a relative density below 0.3 [3]. Foams with a polymer bulk material can be classified as either open or closed cell, depending on how the bulk material is distributed within the microstructure. In an open cell foam, most of the material is concentrated in the struts connecting the vertices of the internal voids. For a closed cell foam, the faces bounded by the struts are closed, fully encompassing the gas within the individual voids. Depending on the bulk material, either plastic yielding or fracture dominates the deformation in rigid foams, while elastic bending dominates the deformation of flexible foams. Rigid foams are often utilized in sandwich structures where the fracture toughness is important [4,5], while flexible foams are more commonly applied in cushioning where recovery is desirable [6]. The different bulk materials do not uniquely yield either rigid or flexible foams, but polyvinyl chloride (PVC) [7] and extruded polystyrene (XPS) [8] are typically found in foams classified as rigid, while polyurethane (PU) is found in foams that are more flexible. For impact mitigation, semi-flexible expanded polypropylene (EPP) [9] and rigid expanded polystyrene (EPS) [10] foams are often utilized, as the combination of good energy absorption and ease of component design and manufacture is desirable.

A typical closed cell foam, such as the EPP foam of the current study, exhibits crushing or cell wall bending during compression, causing a plateau region in the stress-strain curve [3,8]. This allows a comparatively low increase in stress over a large strain interval, which in turn translates to good energy absorption capability, coupled with relatively low stresses.

Polymers are typically rate dependent and, by extension, so are foams [11,12]. Rate dependence of different polymer foams has already received some attention, where quasi-static and low strain rates are typically tested using a traditional electromechanical or hydraulic test machine [13,14]. Intermediate strain rates can be tested using high inertia test machines, for example drop towers, and high strain rates can be achieved using a Split-Hopkinson Pressure Bar (SHPB) [15,16]. The automotive industry, for example, uses foam extensively in the development of pedestrian impact solutions where a range of impact velocities are expected.

Generally, polymers are also sensitive to changes in temperature. Semi-crystalline polymers, such as polypropylene (PP), typically show a

* Corresponding author.
E-mail address: daniel.t.morton@ntnu.no (D.T. Morton).

https://doi.org/10.1016/j.mtcomm.2020.100917
Received 18 September 2019; Received in revised form 10 January 2020; Accepted 10 January 2020
Available online 14 January 2020

significant stepwise reduction in Young's modulus going from the glass transition temperature to the melting temperature [17]. The influence of temperature on different polymeric foams has been investigated in several studies [1,10,18,19]. Zhang et al. [12] investigated EPP foam and found a strong temperature dependence, which will affect the energy absorption capability of a component. Other foams, such as EPS, exhibit less sensitivity to temperature [10]. Polymer foams used in outdoor applications, such as helmets and car bumpers, can be subjected to a large range of temperatures and it is important to understand the effect of temperature on the mechanical response.

EPP foam is an example of a closed cell foam material that is currently used for protective applications, for instance in cars. The dominant loading mode is usually compression when used as an energy absorber. However, other modes such as tension and shear are also present in a realistic impact scenario, for example if bending is seen. The tensile stress-strain response for one type of EPP has been reported by Donnard et al. [20], while other defining qualities such as failure stress and failure strain at room temperature and low loading rates often are reported directly by the manufacturer.

An accurate material description is an important part of utilizing numerical tools in engineering, for example precision FE analyses. Hence, attention must be paid to the acquisition of material data, including the true stress-strain response during the entire deformation domain of interest. Volume is not conserved during the deformation process of a foam and it is, therefore, important to measure the transverse strain of a sample subjected to uniaxial loading to calculate the true stress. Digital image correlation (DIC) has become the primary tool for determination of in-plane or 3D strain fields during material testing of polymers. Considering EPP, Maheo et al. [13], Donnard et al. [20] and Yang et al. [21] have used DIC to determine various measures of Poisson's ratio or transverse contraction. In addition, using DIC, Tang et al. [22] investigated PS foam in three point bending, whereas Senol and Shukla [23] studied hydrostatic compression of PVC. An obvious challenge is to perform tests at various temperatures in combination with instrumentation, for example digital camera(s), for subsequent DIC analysis. Johnsen et al. [24] solved this problem by using a transparent temperature chamber made of polycarbonate.

The aim of this paper is to highlight the differences in mechanical properties, in both compression and tension, between two EPP foams of similar density, as well as quantifying the strain rate and temperature dependence of key qualities defining the mechanical response of the foam. These results will help the engineer tailor the mechanical response of a component by emphasizing the influence of the microstructure of foams with a similar topological structure, and further stress the importance of the environmental conditions an EPP component might experience. Furthermore, the experimental results can be used as the basis for identifying the parameters of material models used in finite element simulations.

2. Materials and experimental procedures

The EPP foams for this study were provided by two different car companies, supplying original equipment manufacturer components denoted Component A and Component B. Material from these two components, Foam A and Foam B, were subjected to an array of compressive and tensile tests under different conditions.

2.1. Materials

EPP foam components are generally comprised of smaller beads, molded into shape. Polypropylene (PP) pellets are pressurized and expanded into foamed beads, typically measuring 2-5 mm in diameter. These beads are then further expanded within a mold where higher temperatures allow the PP to melt, sintering the beads in the final shape of the component [25], as seen in Fig. 1. The components A and B are shown in Fig. 2 along with the respective locations for extraction of

Fig. 1. Example of sintered expanded polypropylene beads in a component.

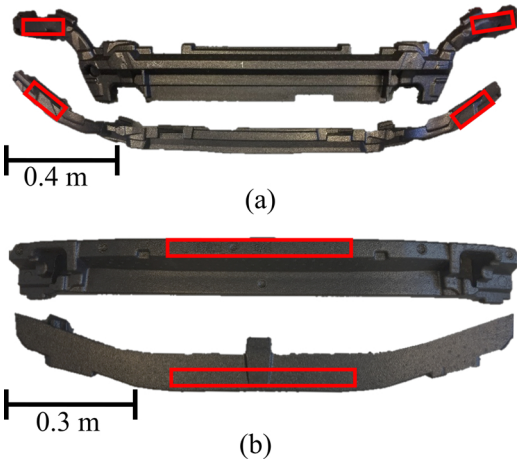

Fig. 2. Sample extraction location from (a) Component A and (b) Component B.

samples. These sample extraction locations were chosen to provide as uniform specimens as possible. After extracting prismatic samples, the density of Foam A and B was estimated by recording the weight of the samples and measuring the distance between the opposing faces using a caliper. The average density of samples from Component A was found to be 28.0 kg/m^3 with a standard deviation of 0.7 kg/m^3. The density of samples from Component B was slightly higher, at 31.3 kg/m^3 with a standard deviation of 1.6 kg/m^3.

Cubic samples measuring $30 \times 30 \times 30$ mm^3 from Foam A and $25 \times 25 \times 25$ mm^3 from Foam B were used for compressive tests. The geometry of Component B restricted the sample size when extracting the desired number of samples for the compressive test program. A small number of larger samples, measuring $37 \times 37 \times 37$ mm^3, and smaller samples, measuring $25 \times 25 \times 25$ mm^3, from Foam A were tested in compression to check for size effects. Longer samples measuring $30 \times 30 \times 60$ mm^3 and $30 \times 30 \times 50$ mm^3 from Foam A and foam B, respectively, were used for the tensile testing. All samples were extracted using a band saw. The exact dimensions were measured with a sliding caliper prior to each test.

2.2. Scanning Electron Microscopy (SEM)

Since the two materials have similar nominal density, but appear to have different mechanical response, it is of interest to compare the internal microstructure of the two foams. To obtain a representative cross section for imaging, rectangular samples were notched on one side, using a knife, and cooled in liquid nitrogen. The samples were broken by bending, while frozen, in order to reduce any potential plastic deformation in the fracture region and provide a surface with minimal damage. The broken samples were subsequently coated with gold using sputter deposition. These coated samples were then imaged

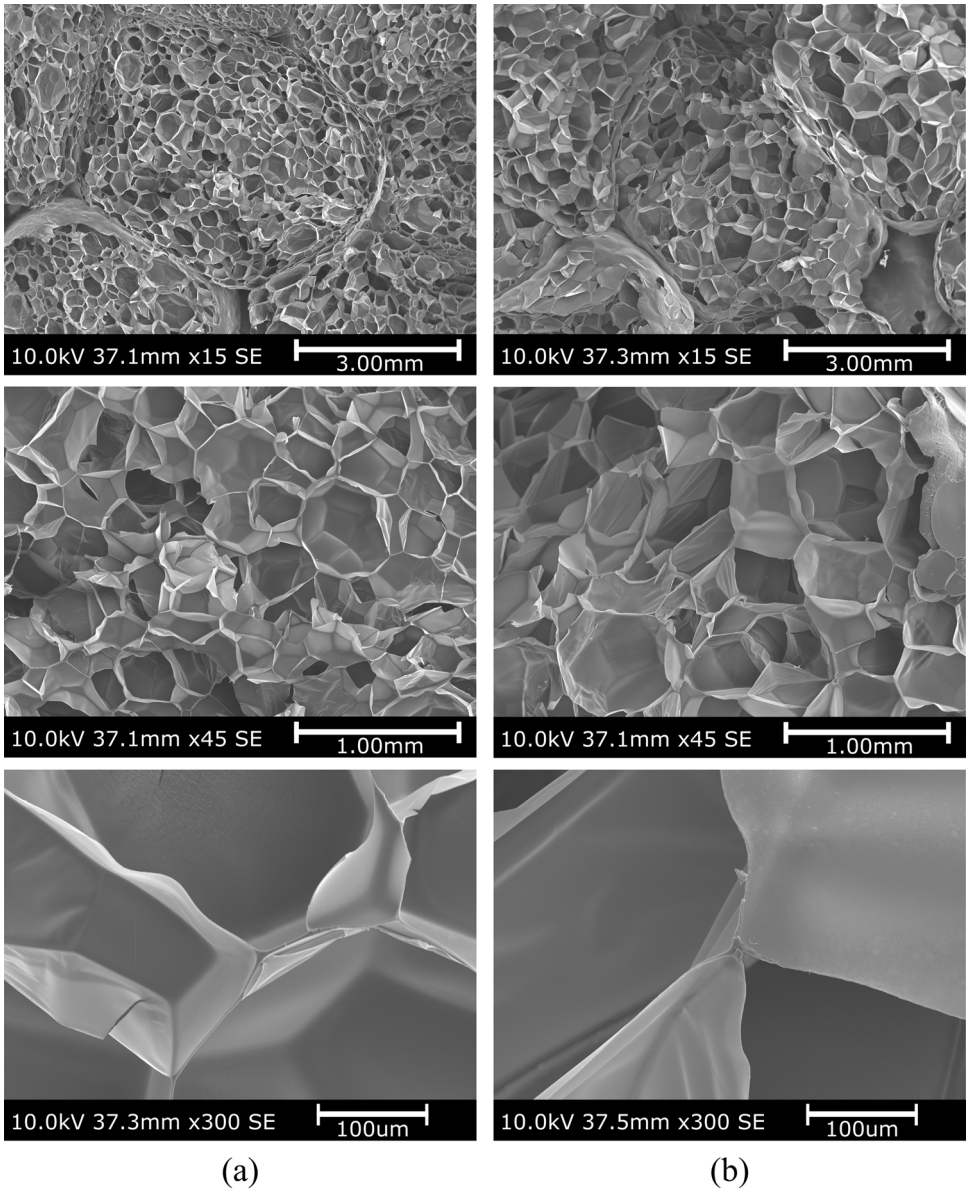

Fig. 3. SEM images of (a) Foam A and (b) Foam B at different zoom levels (×15, ×45 and ×300).

at different magnifications with a Hitachi S-3400 N SEM.

SEM images of Foams A and B are shown in Fig. 3. At the lowest magnification (×15), it is possible to see the individual beads which comprise the foam component. The internal cellular structure of the beads appears more clearly at the two higher magnifications (×45 and ×300).

Comparing the two foams, Foam A has more voids per cross sectional area. As the cells could be broken at different levels across its height, it is not feasible to infer a cell volume or diameter directly from the images, although it is possible to quantify the morphological difference between the two foams. For a selected region within a bead having a known cross-sectional area, the number of voids was counted manually. Foam A had 117 voids in a 6.13 mm^2 area, equating to 19.1 voids/mm^2, while Foam B had 58 voids in a 7.17 mm^2 area, equating to 8.1 voids/mm^2. By extension, the average cell volume and strut length will be smaller in Foam A than in Foam B. At the highest zoom level, it is also possible to see that some of the bulk material is located in the struts of the cells, not just in the cell walls. Unfortunately, the images do not allow establishment of the wall thickness for a representative set of cell walls. This could have helped determine the distribution of material within the structure. It is noteworthy that the region close to the bead walls seems to contain smaller cells. The degree to which the material is located in the bead walls, as opposed to evenly distributed internally in the bead, could also affect the compressive strength. Other studies using X-ray computed tomography also report an increased density in the bead boundaries [26,27].

2.3. Program for compression and tension testing

Foam A and Foam B were tested in compression at different strain rates, while the temperature testing was limited to Foam A. The test matrices for the strain rate and temperature tests are provided in Table 1 and Table 2, respectively. The number of replicate tests is given in parentheses. A total of 72 tests were carried out on Foam A and 16 tests on Foam B.

2.4. Procedures for compression and tension testing

The compression tests were conducted under displacement control at constant crosshead velocity in either an Instron 5980

Table 1
Test matrix (with number of tests) on Foams A and B at different initial strain rates, at room temperature $T = 23°C$

Strain rate, $\lvert\dot{\varepsilon}\rvert$	$10^{-3}s^{-1}$	$10^{-2}s^{-1}$	$10^{-1}s^{-1}$	$10^{0}s^{-1}$
Compression	A (3) B (6)	A (3) B (2)	A (4) B (3)	A (3) B (2)
Tension	A (3) B (3)	—	—	—

Table 2
Test matrix (with number of tests) on Foam A at different temperatures, at initial strain rate $\lvert\dot{\varepsilon}\rvert = 10^{-3}s^{-1}$

Temperature, T	− 30°C	− 20°C	− 10°C	0°C	10°C	23°C	40°C	60°C
Compression	A (4)	A (4)	A (4)	A (3)	A (3)	A (3)	A (4)	A (4)
Tension	A (3)	A (2)	A (4)	A (3)	A (4)	A (5)	A (6)	A (2)

electromechanical test machine (ETM) with a 20 kN load cell, or in an Instron 5944 ETM with a 2 kN load cell. The crosshead velocity, v, is defined by $v = \dot{\varepsilon}L_0$, where $\dot{\varepsilon}$ is the desired initial engineering strain rate and L_0 is the length of the sample. The different initial engineering strain rates are given in Table 1. The deflection of the smaller testing machine was measured to be between 1.74 and 2.20×10^{-4} mm/N. The influence of the machine stiffness is small but has been accounted for in the strain measure derived from the machine displacement. Fig. 4(a) shows the compression test setup. The cubic samples were placed between rigid platens in the test machine. No grease or other friction reducing material was used on the contact interfaces.

The tensile tests were all conducted using the Instron 5944 ETM with a 2 kN load cell. The setup is shown in Fig. 4(b). These tests were also run with a constant crosshead velocity. The fixture of the tensile samples is illustrated in Fig. 4(c). The prismatic samples were bonded to aluminum cubes, which were attached to the test machine with two pins to ensure that no bending moments were present. Loctite Super Glue All Plastic was applied to the end of the tensile samples. This adhesive was allowed to cure before applying Loctite Power Epoxy Universal 5' to the Super Glue infused surface and mounting the aluminum cubes.

Most experiments were monitored with either one or two digital cameras. A speckle pattern was applied to the surfaces of the samples which allowed the use of digital image correlation (DIC). The acquisition rate of the cameras was set to capture between 5 and 10 frames per 1% of deformation (0.5-1 Hz at initial strain rate $\lvert\dot{\varepsilon}\rvert = 10^{-3}s^{-1}$). In the case of the two highest strain rates, the maximum camera acquisition rate of 15 Hz was used.

For temperature testing, the smaller Instron 5944 ETM was fitted with a polycarbonate chamber [24] having small attachments for injection of liquid nitrogen or hot air. The environment below room temperature was controlled by a thermocouple temperature sensor coupled to a Eurotherm 2216e temperature controller that facilitated the release of liquid nitrogen into the chamber. Temperatures above 23°C were obtained with a manually adjustable heat gun attached to the chamber. The same thermocouple sensor monitored the higher temperatures. The samples were conditioned in the temperature chamber for 15 to 30 minutes prior to testing, depending on the desired temperature. The chamber along with the compression and tension test setups is seen in Fig. 4(a) and (b).

3. Experimental results

3.1. Stress and strain measures

Using the element-based DIC software eCorr [28,29], the local logarithmic strain field was established for the tests instrumented with one or two cameras. An example of the logarithmic strain field in compression at four different deformation levels is displayed in Fig. 5. These strains are taken directly from the element mesh of eCorr. The compressive deformation localizes in several bands that span the width

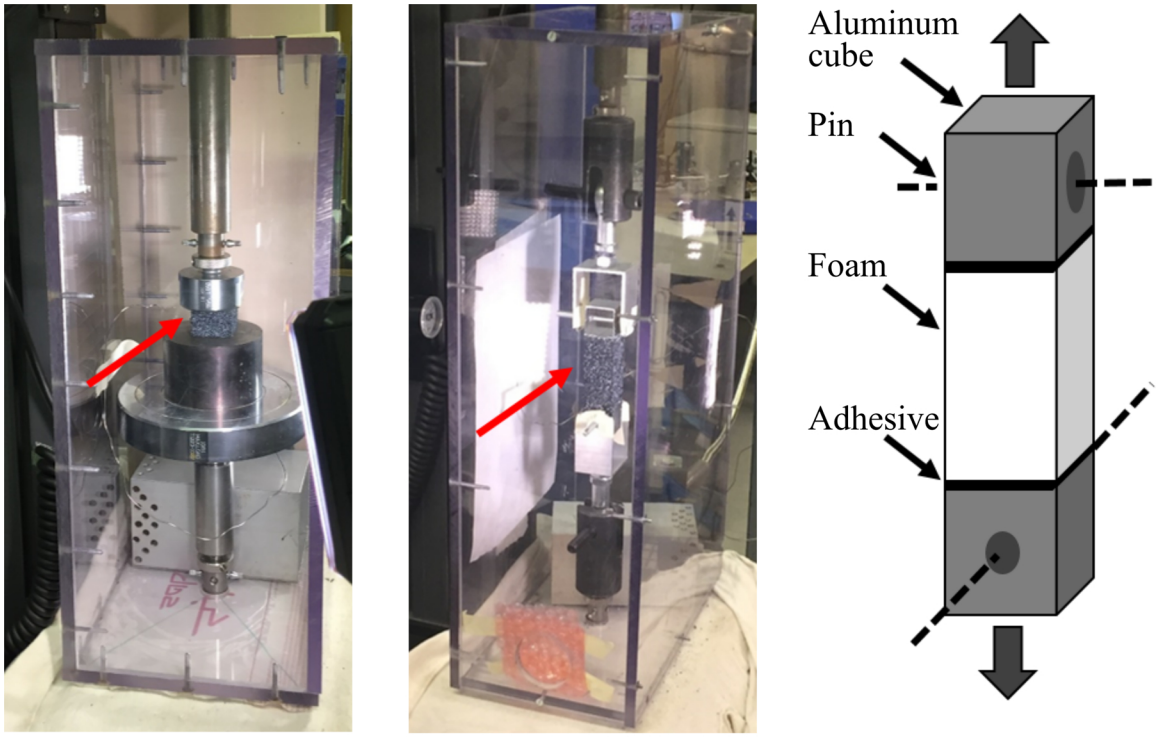

Fig. 4. (a) Compression and (b) tension test setups including the temperature chamber, and (c) illustration of the tension test fixture. The arrows in (a) and (b) point to the specimens.

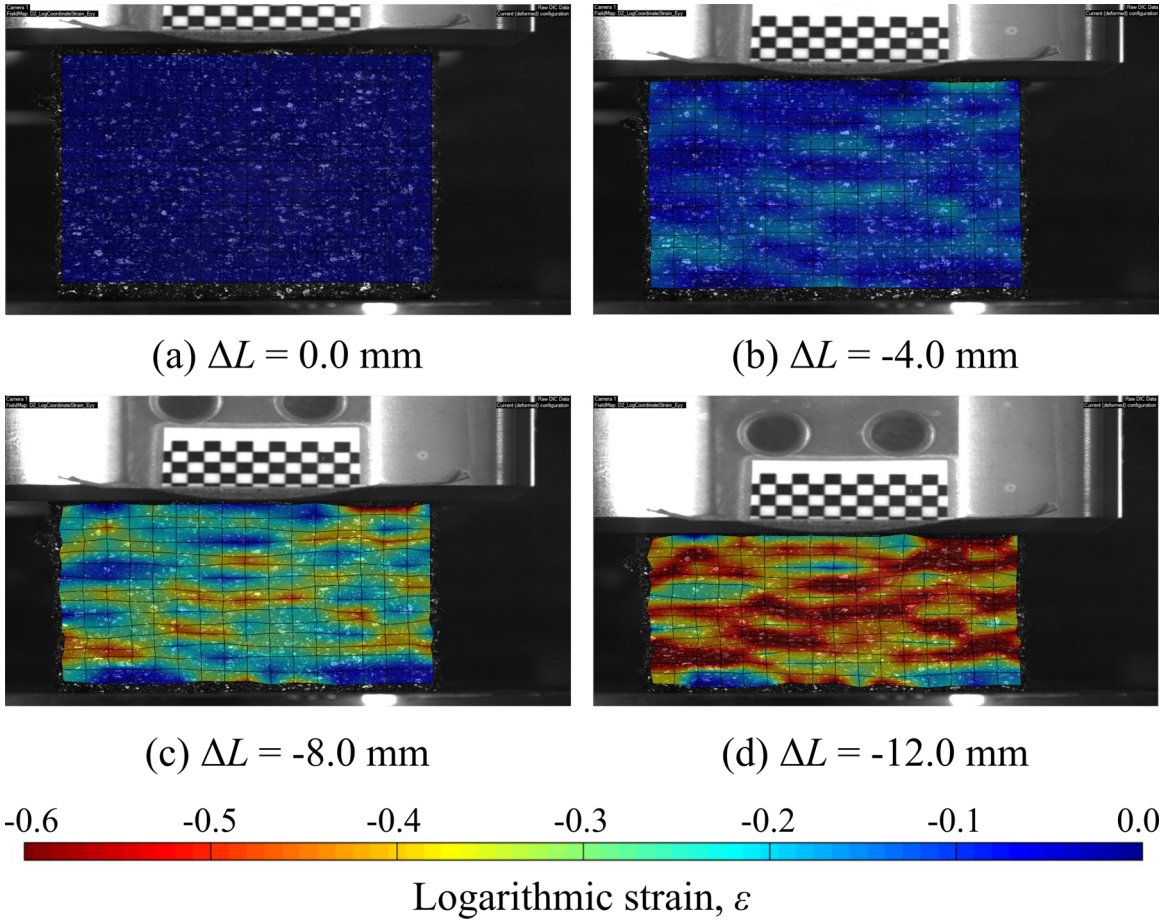

Fig. 5. Field map of the local longitudinal logarithmic strain, in compression, of Foam A at different deformation levels (L_0 = 30.6 mm).

of the sample. It appears from the test data that the evolution of these bands defines the plateau region of a typical stress-strain curve.

Fig. 5 demonstrates that the strains vary considerably between the elements in the DIC mesh. These strains are, therefore, not suitable for application in a stress-strain curve for the foam material, and an average strain measure is required. One convenient choice is to apply the machine displacement and define a global strain measure taking the entire length of the sample into account. This global logarithmic strain ε is calculated as

$$\varepsilon = \ln\left(1 + \frac{\Delta L}{L_0}\right) \tag{1}$$

where L_0 is the initial length of the sample, and the change in length ΔL is determined from the crosshead displacement of the test machine. The sign of ΔL is negative in compression.

While the global strain uses the initial length of the sample and the crosshead displacement of the test machine, the DIC displacement field can also be employed in the calculation of a representative logarithmic strain for the compression tests. Hereafter referred to as the DIC strain, this measure is derived from the average engineering strain $\bar{e}$ of several longitudinal virtual extensometers placed across the width of the DIC mesh, viz.

$$\varepsilon = \ln(1 + \bar{e}) \tag{2}$$

The average engineering strain is calculated from

$$\bar{e} = \frac{1}{n}\sum_{i=1}^{n} \frac{\Delta L_i^v}{L_{0,i}^v} \tag{3}$$

where n is the number of virtual extensometers and ΔL_i^v is the change of length of extensometer i. The initial length $L_{0,i}^v$ of each extensometer is typically around 5 mm shorter than the full length of the sample. If the test featured two cameras, the reported strain is the average of the strains from both cameras.

Considering the tensile loading mode, the global strain measure is not applicable because the crosshead displacement of the machine also incorporates deformation of the fixtures, see Fig. 4(c). Thus, the data from the tensile tests rely only on the strain measure from the DIC and virtual extensometers, and Eq. (2) is used to calculate the strain.

A useful deformation measure is the incremental contraction ratio

$$\nu = -\frac{d\varepsilon_t}{d\varepsilon} \tag{4}$$

where $d\varepsilon_t$ is the transverse strain increment and $d\varepsilon$ is the longitudinal strain increment. According to Pierron [30], describing the contraction ratio as a function of the incremental, rather than total, strain allows a more detailed description of the evolution of ν at large deformations because small changes in transverse strains are not smoothed by a large longitudinal strain.

Fig. 6 shows the incremental contraction ratio ν as a function of strain for both foams and in both loading modes at room temperature and an initial strain rate of $10^{-3}s^{-1}$. The difference between the transverse strains in tension relative to compression is significant, and is assumed to arise from the cell walls buckling and a shrinking internal void volume in compression, contrary to cell wall stretching in tension. Clearly, the transverse expansion is close to zero in compression, and the slight auxetic behavior observed at large compressive strains could be a result of friction between the sample and compression platens. Neglecting this small auxetic effect, the true stress in compression is well approximated by the engineering stress, so that

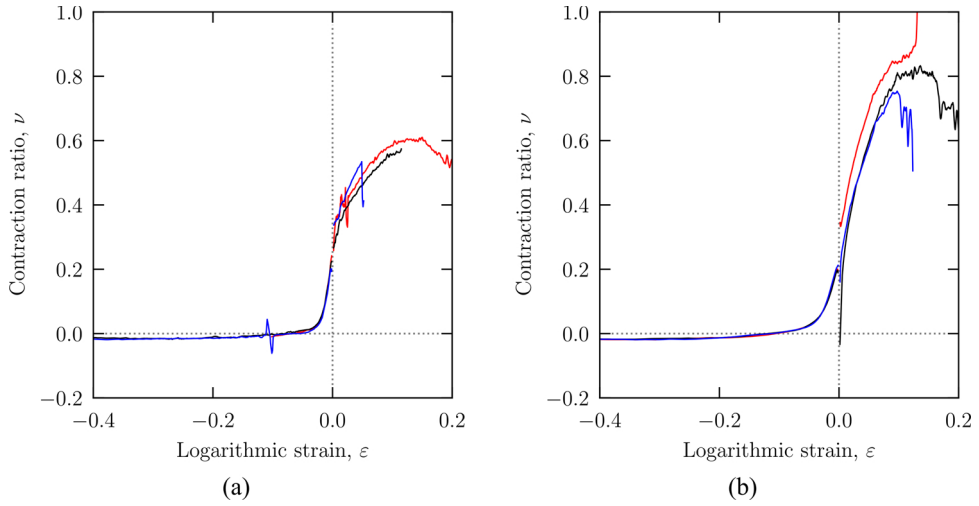

Fig. 6. Contraction ratio as a function of logarithmic strain for (a) Foam A and (b) Foam B for three repeat tests in both compression and tension (T = 23°C, $|\dot{\varepsilon}| = 10^{-3}\text{s}^{-1}$).

$$\sigma \approx \frac{F}{A_0} \tag{5}$$

where F is the load and A_0 is the cross section area of the undeformed specimen. However, in tension the transverse contraction is large, see Fig. 6, and therefore it must be included in the calculation of the true stress in tension, as prescribed by

$$\sigma = \frac{F}{A_o(\bar{\lambda}_t)^2} \tag{6}$$

where $\bar{\lambda}_t$ is the average transverse stretch. Again, several virtual extensometers are applied, now placed transversely to the loading direction. The initial length of each of these transverse extensometers is $W^v_{0,i}$ and ΔW^v_i is the corresponding change of length. The average transverse stretch is hence found as

$$\bar{\lambda}_t = 1 + \frac{1}{n}\sum_{i=1}^{n}\frac{\Delta W^v_i}{W^v_{0,i}} \tag{7}$$

The difference between the global and DIC strain measures in compression is illustrated by the stress-strain curves in Fig. 7, where a sample from Foam A was tested at room temperature with a quasi-static strain rate $|\dot{\varepsilon}| = 10^{-3}\text{s}^{-1}$. It appears from the figure that the initial, elastic part of the curve is steeper when the DIC strain measure is applied. The difference between the curves is probably caused by end and surface effects of the sample. The surfaces experienced some damage due the sawing during sample extraction. The material close to the ends is not included in the DIC strain measure since the virtual extensometers are around 5 mm shorter than the specimen. The two stress-strain curves do, however, converge when the logarithmic strain exceeds approx. 0.2. The longitudinal strain in compression approaches 2 in this study and, with exception of the initial stiffness, the two strain measures are, therefore, equivalent for practical purposes. Thus, only strains calculated from the machine displacement are used in the compressive stress-strain curves hereafter.

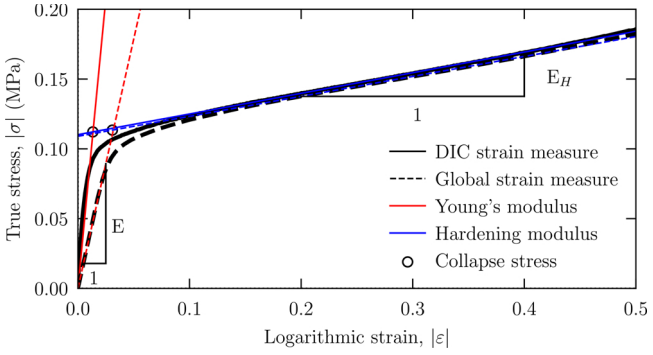

Fig. 7. Stress-strain curve based on local (DIC) or global strain measure in a compression test on Foam A, and definitions of Young's modulus E and the hardening modulus E_H. The collapse stress σ_c is defined as the intersection between the two lines defining E and E_H.

From either the DIC strain measure or the global strain measure, it is possible to derive relevant quantitative parameters defining the foam response. Referring to Fig. 7, the selected parameters include the initial stiffness, commonly referred to as the Young's modulus (E), the collapse stress (σ_c) and the hardening modulus (E_H). Young's modulus is the slope of the initial part of the stress-strain curve. For consistency, the slope is evaluated at the stage corresponding to the inflection point of the force-displacement curve, as this curve typically has a slight S-shape. The hardening modulus is found by evaluating the slope of the stress-strain curve at the point where the force- displacement curve reaches its second inflection point. This occurs in the middle of the plateau region, and the hardening modulus is also referred to as the plateau stress modulus in the literature. The collapse stress σ_c refers to the stress at which the foam deforms with little increase in stress as strain increases. Following Bouix et al. [15], σ_c is defined as the intersection between the two lines with slope E and E_H in Fig. 7. Henceforth, Young's modulus from both strain measures will be presented if available, while the collapse stress and hardening modulus will be derived from the global strain, as these values do not differ significantly from the DIC strain measure.

During initial testing of the samples with different sizes, the larger samples 37 × 37 × 37 mm^3 from foam A exhibited a slightly higher (10%) collapse stress than the smaller 25 × 25 × 25 mm^3 samples, but the large specimens also had a slightly higher (7%) density. Similar trends were seen by Cronin and Ouellet [16]. Within each test configuration, little scatter was seen between repeat tests. For example, the collapse stress at room temperature and quasi-static loading of Foam A lies within ± 3.5% of the mean collapse stress.

Initial testing also established that samples taken from the components exhibited isotropic behavior if extracted sufficiently far (3 mm) from the component surface. It was observed that samples extracted close to the surface of the component had a slightly higher collapse stress in the direction normal to the component surface. According to Bouix et al. [15], the density of EPP can be higher close to the component surface, which will influence the sample response, but this effect has not been quantified in the present study. From initial studies of

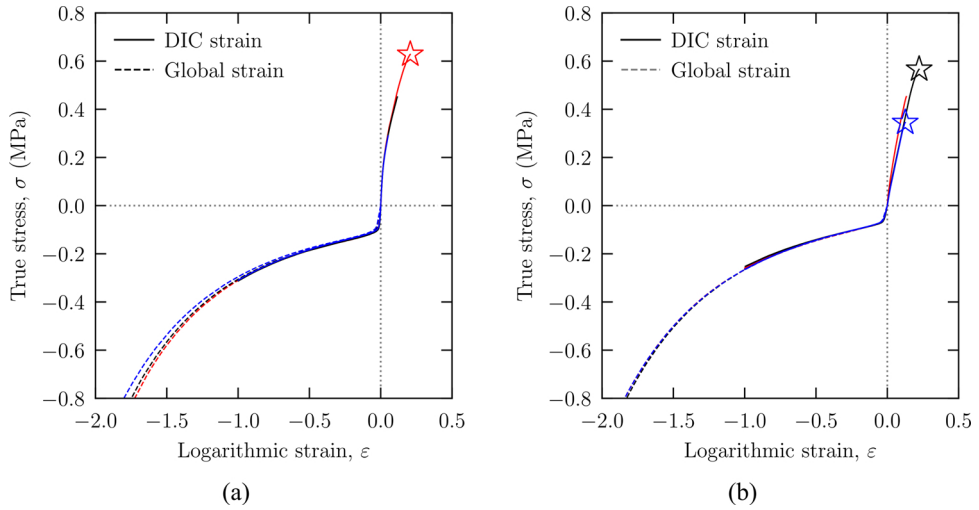

Fig. 8. Stress-strain curves for (a) Foam A and (b) Foam B for three repeat tests in both compression and tension (T = 23°C, $|\dot{\varepsilon}| = 10^{-3}s^{-1}$).

Component A, the sample extraction location does not significantly influence the mechanical response beyond the slight difference caused by surface effects.

The stress-strain curves of the two foams, in both loading modes, are shown in Fig. 8. The compressive samples of Foam A and B measured $30 \times 30 \times 30\,mm^3$ and $25 \times 25 \times 25\,mm^3$, respectively, while the tensile samples measured $30 \times 30 \times 60\,mm^3$ and $30 \times 30 \times 50\,mm^3$. The test conditions are room temperature and a strain rate of $10^{-3}s^{-1}$, and the figure reports three tests in both tension and compression. It is seen that the materials exhibit a typical collapse response in compression, with a pronounced plateau region. It appears that Foam A has a higher collapse stress than Foam B in compression. The stress in tension, on the other hand, is continuously increasing. The compression tests were terminated by either a fixed displacement limit or the load cell load limit of 2 kN, depending on the test setup. The tensile tests were terminated after a large reduction in load. This reduction was usually caused by failure of the foam, but some samples failed in the bonding interface prior to material failure. Fig. 9 shows some of the tensile samples tested at different temperatures, where some have failed in the bonding interface. The stress-strain curves of the samples where tensile failure occurred in the foam, not at the bonding interface, are terminated with stars.

3.2. Strain rate dependence

For evaluation of the strain rate dependence, both foams were tested in compression at engineering strain rates $|\dot{\varepsilon}| = 10^{-3}$, 10^{-2}, 10^{-1}, $10^{0}s^{-1}$. All these tests were carried out at room temperature, see Table 1. The stress-strain curves for Foam A and B are shown in Fig. 10(a) and Fig. 10(b), respectively. It appears from the figures that both foams exhibit significant strain rate sensitivity. There is also some scatter between replicate tests, particularly at higher compressive strains.

From the curves in Fig. 10, it is possible to determine the two moduli, E and E_H, and the collapse stress, σ_c. The resulting parameters are plotted as a function of strain rate in Fig. 11. The collapse stress of the two foams exhibits similar increase with increasing strain rate, but the stress levels are different, as seen in Fig. 11(a). The hardening modulus of the two foams, seen in Fig. 11(b), is similar in size, but the strain rate sensitivity differs. Young's modulus derived from the global strain measure, in Fig. 11(c), appears to be relatively constant, but with high scatter. The other measure of Young's modulus, derived from the local strain field, is included in Fig. 11(d). Limited camera frame rate at high compression speeds caused large displacements between each frame, and reliable local strain fields at higher strain rates could not be established. Nevertheless, the different scales of the vertical axes in Fig. 11(c) and 11(d) reveal that the local DIC strain yields a significantly higher estimate of E than the global machine strain does. The numerical values from the graphs in Fig. 11 (a), (b) and (d) have been summarized in Table A1 in Appendix A.

3.3. Temperature dependence

The mechanical response of Foam A at different temperatures was tested in both compression and tension at a strain rate of $10^{-3}s^{-1}$, see Table 2. The temperatures ranged from − 30°C to 60°C. The stress-strain curves in compression are shown in Fig. 12, while Fig. 13 displays the stress-strain curves in tension. Generally, the response has a strong dependence on temperature, where Young's modulus and the collapse stress in compression increase with decreasing temperature. A similar trend is apparent in the tension tests.

As with the strain rate tests, key parameters of the mechanical response at different temperatures can be extracted from the compression test data. The different qualities are plotted in Fig. 14. Using room temperature as reference, the collapse stress shown in Fig. 14 (a) increases by approximately 110% at − 30°C and decreases by approximately 50% at 60°C. The consequence of this difference is a significant change in energy absorption between the highest and lowest temperatures. The hardening modulus plotted in Fig. 14(b) is also temperature dependent, but to a lesser degree than the collapse stress. Young's modulus also varies with temperature, see Fig. 14(c) and 14(d). The numerical values from the graphs in Fig. 14 (a), (b) and (d) have been

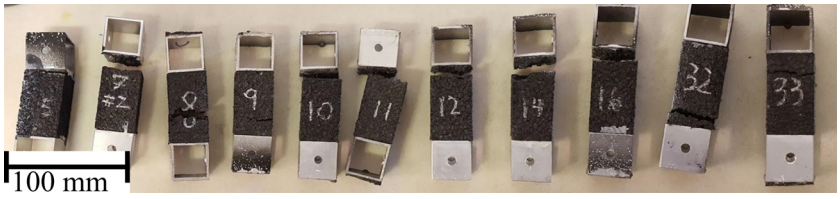

Fig. 9. Samples tested in tension at different temperatures. Sample 8 illustrates failure within the material, while sample 10 is an example of bonding failure.

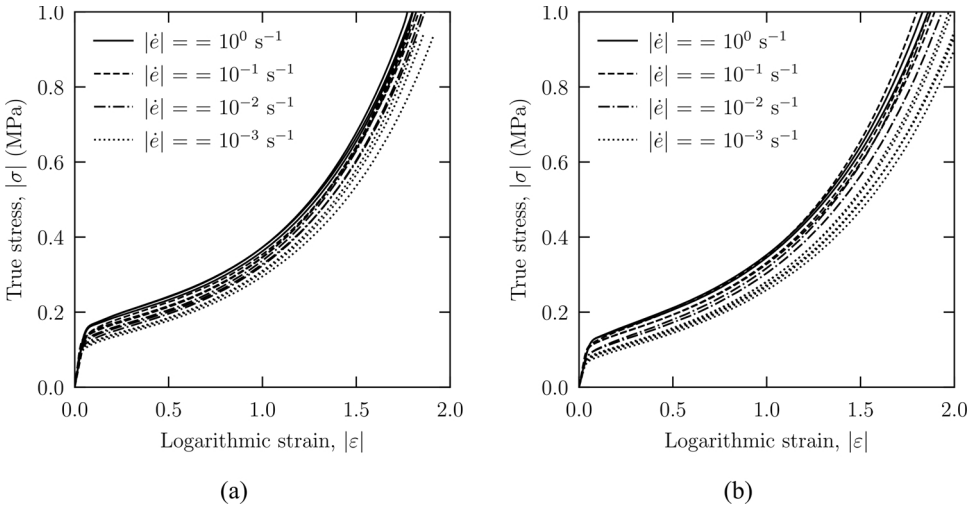

Fig. 10. Stress-strain curves at different strain rates in compression for (a) Foam A and (b) Foam B (T = 23°C).

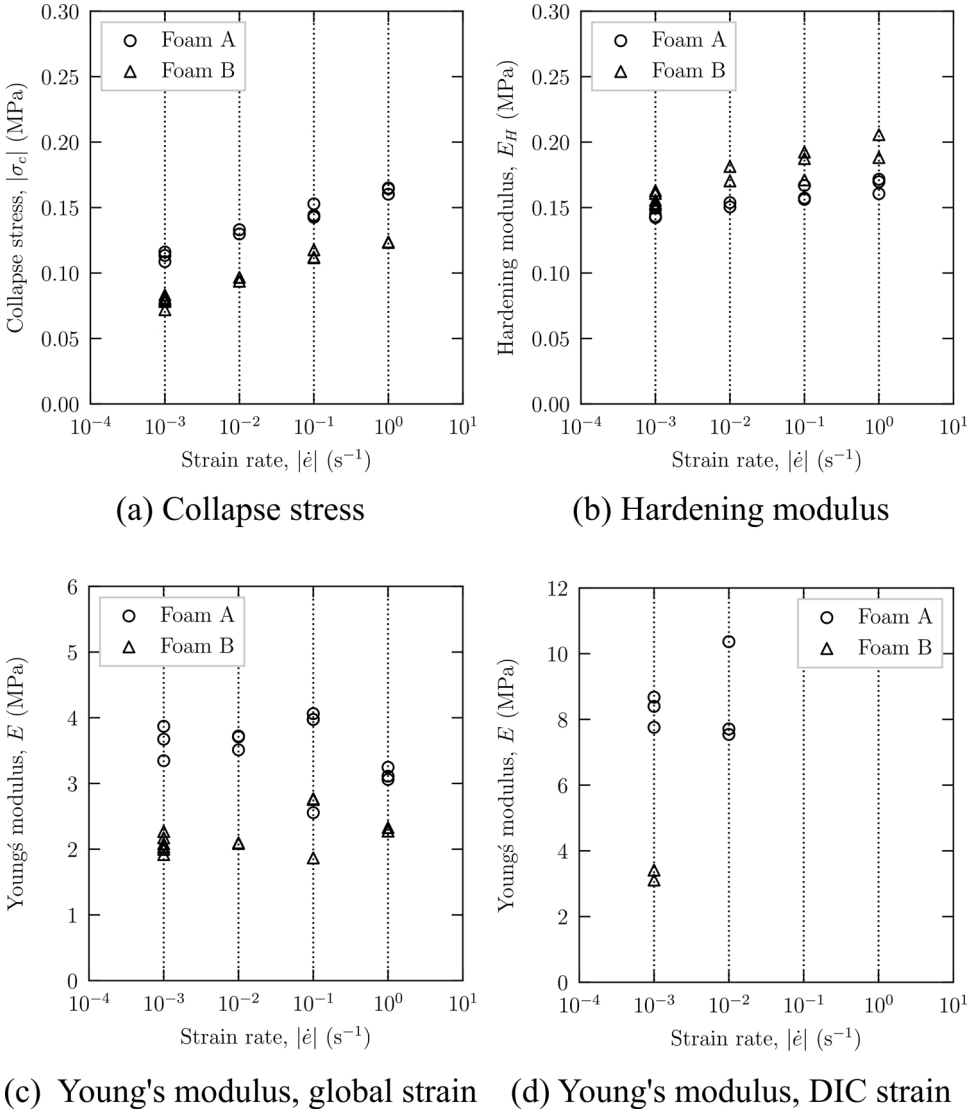

Fig. 11. Material parameters at different strain rates in compression (T = 23°C).

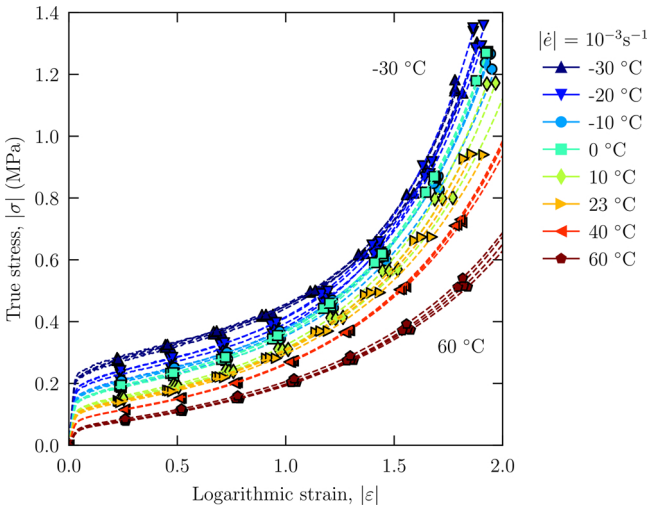

Fig. 12. Stress-strain curves at different temperatures in compression for Foam A ($|\dot{\epsilon}| = 10^{-3}s^{-1}$).

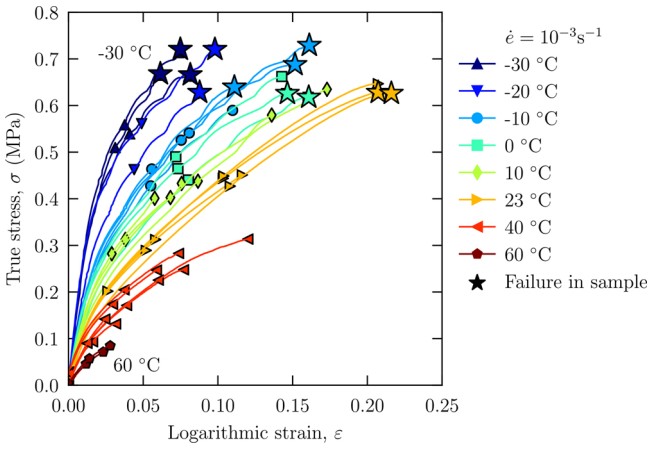

Fig. 13. Stress-strain curves at different temperatures in tension for Foam A ($|\dot{\epsilon}| = 10^{-3}s^{-1}$).

summarized in Table A1 in Appendix A.

4. Discussion

The previous section revealed that the mechanical response of EPP foams is complex, even under simple uniaxial loading conditions. The behavior in compression and tension is substantially different with respect to both the stress-strain curves and transverse deformations. Additionally, the foams exhibit a strong rate sensitivity. For practical applications, the relatively large temperature dependence introduces particular challenges if an EPP foam component is expected to experience a wide range of temperatures.

4.1. Local strain field

The local strain field depicted in Fig. 5 shows localization bands during the compressive deformation. This is probably caused by slight differences in cell morphology, microstructure or density. The data from the local strain field also lends additional weight to the common assumption of foam having low, for all practical purposes zero, transverse expansion in the post-collapse region of the compressive stress-strain curve.

Contrary to the compression tests, the transverse contraction is significant in the tensile tests. The high values of the contraction ratio ν seen in Fig. 6 are facilitated by the transverse collapse of cells and resulting negative volumetric strain (corresponding to $\nu \geq 0.5$). An analogous explanation for this could be the deformation of an ellipse with a fixed circumference. As one axis is elongated, the total area approaches zero as the current minor axis approaches zero length. The transverse contraction in tension will influence the response when modeling mixed loading cases that include bending. Due to geometric constraints of the components shown in Fig. 2, the length of the tensile specimens was limited to twice the width. A shorter sample will have a higher stress triaxiality, due to the test fixture and, by extension, limit the transverse contraction behavior. Longer samples, with lower triaxiality, would allow larger transverse contraction. The samples of the different foams tested in tension are of similar lengths, such that the transverse strain data can be directly compared.

According to Figs. 11(c) and 11(d), there is a significant discrepancy in the compressive Young's modulus E derived from the global and local strain fields. Figs. 14(c) and 14(d) show a similar trend. Comparing the two measures of Young's modulus in Fig. 11 and Fig. 14, it is found that Young's modulus calculated from the machine displacement is between 30% and 50% of Young's modulus from the DIC data. This is assumed to be caused by the method of sample extraction, involving a band saw that damages all sample surfaces. A small region of soft material close to the surface will disproportionately affect the global initial stiffness. Young's modulus derived from the local strain field excludes the damaged outer layer, resulting in a stiffer response. Conversely, when calculating the initial stiffness from the local strain field, the response will depend on any geometrical imperfections of the cube. Typically, two sides are imaged, and the resulting deformation measure derived from each strain field is averaged. If the top and bottom surfaces of the sample are not parallel, the strain on the imaged sides could be different from the average strain, which in turn will affect the value of the initial stiffness.

It is interesting that Young's moduli in tension and compression only differ slightly, see Fig. 14(d). This observation suggests that the physical mechanism governing Young's modulus at a micromechanical level is the same in the two loading modes. Considering the initial elastic domain with reversible deformations, it is probable, therefore, that the major deformation mechanism is elastic bending and stretching of the cell walls and struts. The bending stiffness of the microstructure should, in this case, be comparable in tension and compression. Eventually, the cell walls start to buckle in compression, potentially together with plastic yielding of the struts, resulting in an abrupt change of stiffness when the collapse stress is reached.

4.2. Foam A vs Foam B

Fig. 11(a) shows that the collapse stress of Foam A is more than 40% higher than that of Foam B. A difference in collapse stress between two foam types of different cell size has also been reported by Bouix et al. [15] in tests done on EPP with a density of 90 kg/m^3. They also observed that smaller cell size resulted in a higher collapse stress. The main mechanism causing this discrepancy is not obvious and will be discussed in the following.

Gibson and Ashby [3] proposed a model for 3D closed cell foams. This model can be used to estimate Young's modulus and the collapse stress, based on the morphology of the cells and the properties of the bulk material. Young's modulus E^* of the foam is predicted from

$$\frac{E^*}{E_s} \approx \phi^2 \left(\frac{\rho^*}{\rho_s}\right)^2 + (1-\phi)\frac{\rho^*}{\rho_s} \tag{8}$$

where E_s is Young's modulus of the bulk material, ϕ is the amount of material contained in the struts, relative to the total amount of bulk material in a unit cell, and ρ^* and ρ_s are the foam and bulk material density, respectively. From the same model, the plastic collapse stress $\sigma^*_{c,pl}$ can be estimated by

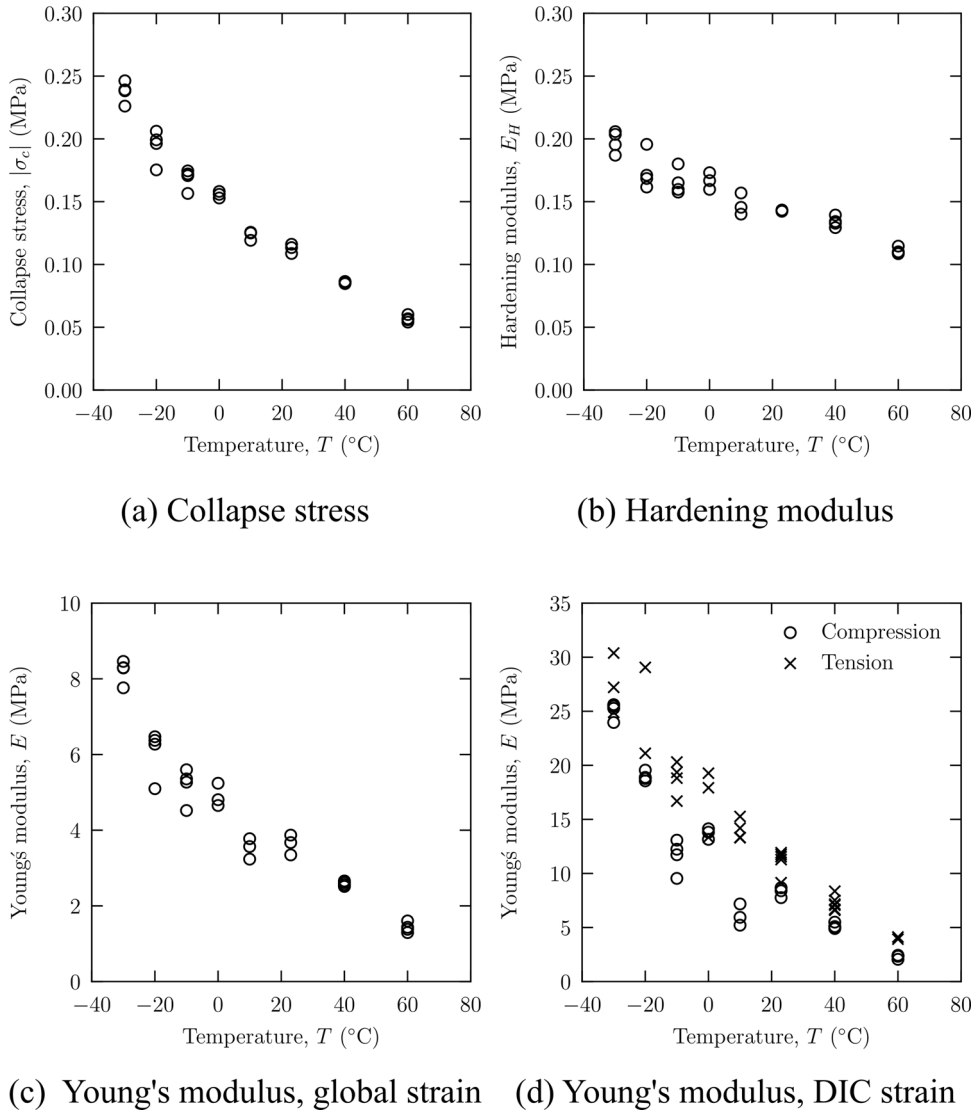

Fig. 14. Material parameters at different temperatures for Foam A.

$$\frac{\sigma^*_{c,pl}}{\sigma_{ys}} \approx 0.3\left(\phi\frac{\rho^*}{\rho_s}\right)^{\frac{3}{2}} + 0.4(1-\phi)\frac{\rho^*}{\rho_s} \tag{9}$$

where σ_{ys} is the yield stress of the bulk polymer. This equation indicates that a higher material concentration in the cell struts results in a reduced collapse stress. The underlying physical mechanism for the plastic collapse stress in Eq. (9) is plastic yielding in the cell walls and struts. An alternative mechanism is elastic buckling of the cell walls. For this case, Gibson and Ashby [3] proposed the following relation for estimation of an elastic collapse stress

$$\frac{\sigma^*_{c,el}}{E_s} \approx 0.05\left(\frac{\rho^*}{\rho_s}\right)^2 \tag{10}$$

Here, the estimated collapse stress is governed only by the relative density of the foam and Young's modulus of the bulk material. The large difference in the collapse stress found between Foam A and Foam B of similar density indicates, either that the above equation might not be applicable, or that the Young's moduli of the two bulk materials are drastically different.

The three equations show that Young's modulus, the elastic buckling stress and the plastic collapse stress are all invariant with respect to the cell size of the foam. If considering elastic buckling, shorter cell walls are less prone to buckling, but the effect is countered by the reduced cell wall thickness and, by extension, the reduced second moment of area.

Even if the mechanical properties of the original PP were known, these might be significantly altered during the subsequent processing. Without the correct Young's modulus or yield stress of the bulk material, it is not feasible to use the above equations to estimate the values of ϕ for the two foams accurately. Assuming the same ϕ for both foams would require the bulk properties to be drastically different. Without information about either the bulk material or ϕ it is difficult to determine the ultimate cause of the large difference between the two foams. Depending on the grade of the PP (homopolymer, random copolymer or block copolymer), the tensile modulus for the unprocessed material is between 900 and 1550 MPa, with random and block copolymers being the softest. The yield stress is typically between 24 and 35 MPa, again with random and block copolymers being the weakest [31]. Additionally, the degree of crystallinity will also affect the final properties. Differential scanning calorimetry (DSC) analysis of the foams used in this study indicate a similar degree of crystallinity if the bulk (reference) material is assumed identical. DSC measures the endothermic heat flow as a function of temperature and can be used to establish the enthalpy of fusion (melting) for a material. Crystallinity is commonly estimated by comparing the enthalpy of fusion for the semi-

crystalline sample with the enthalpy of fusion for a 100% crystalline reference sample [32]. The heat flow as a function of temperature is similar for both materials, resulting in similar crystallinity if the same reference is used. Although the range in mechanical properties of the different grades of PP could explain the discrepancy, EPP from two major suppliers, JSP and BASF, are both made with copolymers [33,34], indicating that the range of mechanical properties might be limited to the case of copolymers. This is further supported by EPP process patents referencing random or block copolymers [25,35]. An alternative approach for finding the bulk material properties could be through inverse modeling using a micromechanical model, if the geometry could be adequately described.

Bouix et al. [15] compared Eq. (9) with experimental results from compression testing of EPP at several densities. They reported good agreement between the observed collapse stress of the quasi-static tests and the theoretical estimate when using $\sigma_{ys} = 48\,\text{MPa}$, $\rho_s = 910\text{kg/m}^3$ and $\phi = 1$. For the two foams at hand, the micrographs in Fig. 3 show notable amounts of material located in or close to the corners of the cells, but $\phi = 1$ would leave zero material in the cell walls as opposed to the struts. Assuming the same bulk material properties for Foam A and Foam B as applied by Bouix et al. [15] and solving Eq. (9) for ϕ, yields $\phi_A = 0.93$ and $\phi_B = 1.02$. The latter number, being outside the range of validity, indicates that either the applied bulk material yield stress is too high, or that most of the material is in fact located in the struts. It is worth noting that the PP yield stress used here, $\sigma_{ys} = 48\,\text{MPa}$, is higher than values commonly found in the literature. Using the lower bound of PP yield stress reported by Tripathi [31] instead, $\sigma_{ys} = 24\,\text{MPa}$, the resulting values of ϕ for Foam A and B are 0.68 and 0.87, respectively. These figures indicate that a significant portion of material is still concentrated in the struts of the cellular structure unless the bulk yield stress is even lower than 24 MPa.

4.3. Rate dependence

In the low to intermediate strain rate regime investigated in this study, see Fig. 10, it is evident that the collapse stress σ_c of the foam is strain rate dependent. The strain rate dependence is expected to be even greater at higher strain rates, as reported in other investigations of EPP [15,16]. In these studies of EPP and other polymeric foams, the stress at a given strain is found to exhibit an initial log-linear dependence on the strain rate before a sharp increase in rate sensitivity occurs at strain rates above 10^2s^{-1}.

In contrast, Young's modulus E does not seem to be strain rate dependent at these low to intermediate rates. This is consistent with data from compression testing of bulk polymer at different strain rates where the initial stiffness of the PP has a seemingly low strain rate dependence for strain rates up to 10^{-1}s^{-1} [36,37]. These studies do, however, show that the yield stress of the bulk polymer is somewhat strain rate dependent, which could indicate that the collapse stress of the foam is influenced by the yield stress of the bulk material. The Gibson-Ashby model in Eq. (9) could then be applicable to the present material.

4.4. Temperature

Young's modulus of different PP bulk materials has been studied by several sources [38,39], and all show a strong temperature dependence comparable to that seen in the present study. Data for the yield stress or failure stress in tension [39,40] also show significant temperature dependence, depending on the type of PP. As both the stiffness and yield properties of bulk PP exhibit strong temperature dependence, it is not possible to isolate either of these effects and explain the main collapse mechanism defining the collapse stress.

According to Fig. 14(d), there is a discrepancy between the compressive and tensile Young's modulus calculated from the local strain field at temperatures between − 20°C and 10°C. The Young's modulus in compression at these temperatures is significantly below the tensile Young's modulus, and one contributing effect could be sample irregularity and non-squareness, which were not captured in the sample measurements. The samples for each temperature were extracted next to one another and at the same time, so any systematic deviation in sample shape could affect samples from the same set. This is supported by the DIC images of the affected tests, where one camera shows a linearly varying longitudinal strain distribution across the sample width. The other camera was imaging the side with the larger compressive strain, partially explaining the lower stiffness resulting from larger surface strain increments than the average throughout the sample.

During tensile testing, the bonding method did not produce optimal results, which is particularly evident in the tests at temperatures of 40°C and 60°C. According to Fig. 13, all specimens failed in the bonded surface at these two temperatures. The super glue seemed to adhere well to the foam, and the adhesion between the epoxy and the super glue was satisfactory. The weak bonding interface was between the epoxy and the aluminum. Bonding agents better suited to the aluminum were tested but were difficult to cure and did not adhere well to the epoxy or super glue. A revised approach could include other bonding agents and/or altered specimen geometry. A more complex geometry could, for example, be achieved by cryogenic machining.

The grade of the bulk PP will also affect the behavior of the EPP foam at different temperatures. The glass transition temperature of PP plays a major role. The brittle temperature of PP ranges from − 10°C to 15°C for random copolymers and − 40°C to 10°C for block copolymer [31], which could affect the final response of the foam. However, comparing the response at the low temperature levels in Figs. 12 and 13, there are no obvious indications of far more brittle behavior at − 30°C than at 0°C. Therefore, it seems that the glass transition temperature of the bulk PP is well below 0°C.

5. Concluding remarks

The experimental study shows strong effects of strain rate and temperature on the stress-strain response of the foams investigated. The observed difference in the mechanical response between the two foams of similar density indicates that tuning of the microstructure could be used to acquire desired properties. Between the two tested foams, the nominal density is similar but the collapse stress of the stronger foam under quasi-static loading conditions is more than 40% higher than that of the weaker foam. From the SEM images, the stronger foam is seen to have a finer cellular structure, with smaller cells. The strain rate dependence at low and intermediate strain rates is significant and will be relevant when considering energy absorption in impact mitigation. The collapse stress increases by 45% for Foam A and 57% for Foam B at a strain rate of 10^0s^{-1} relative to a quasi-static strain rate of 10^{-3}s^{-1}. It is also evident that the operating temperature of EPP foam components should be considered in the product development process, as different temperatures strongly alter the behavior. Relative to room temperature conditions, the collapse stress increases by approximately 110% at the coldest temperature (− 30°C) and decreases by 50% at highest temperature (60°C). Further studies of the mechanical properties of EPP would benefit from more information on the bulk material, preferably material which has undergone the same temperature and environmental history.

Declaration of interests

The authors declare that they have no known competing financial interests or personal relationships that could have appeared to influence the work reported in this paper.

CRediT authorship contribution statement

Daniel T. Morton: Methodology, Investigation, Visualization, Writing - original draft. **Aase Reyes:** Conceptualization, Methodology, Supervision, Writing - review & editing. **Arild H. Clausen:** Conceptualization, Methodology, Supervision, Writing - review & editing. **Odd Sture Hopperstad:** Conceptualization, Methodology, Supervision, Writing - review & editing.

Acknowledgements

The present work has been carried out with financial support from Centre of Advanced Structural Analysis (CASA), Centre for Research-based Innovation, at the Norwegian University of Science and Technology (NTNU) and the Research Council of Norway through project no. 237885 (CASA). The authors would like to acknowledge Dr. Egil Fagerholt, Mr. Trond Auestad, Mr. Ruben Sælen, Mr. Jonas Rudshaug, Mr. Torodd Lønning and Mr. Tore Wisth for assistance with the experimental program. Furthermore, thanks are given to Dr. Frode Grytten for assistance with the DSC analysis.

The raw/processed data required to reproduce these findings cannot be shared at this time as the data also forms part of an ongoing study.

Appendix A

Table A1
Summary of Fig. 11 (a), (b) and (d), Fig. 14 (a), (b) and (d), and the ultimate failure stress in tension, σ_{max}.

Strain rate $\lvert\dot{\varepsilon}\rvert$ [s^{-1}]	Temp. T [°C]	Collapse stress σ_c [MPa]		Hardening modulus E_H [MPa]		Young's modulus (DIC) E_{DIC} [MPa]			Fail. stress σ_{max} [MPa]
		Compression		Compression		Compression		Tension	Tension
		Foam A	Foam B	Foam A	Foam B	Foam A	Foam B	Foam A	Foam A
10^{-3}	23	0.116	0.078	0.142	0.150	8.68	–	–	–
		0.113	0.081	0.143	0.163	8.40	3.41		
		0.109	0.072	0.143	0.155	7.76	3.11		
			…		…		…		
10^{-2}	23	0.130	0.097	0.150	0.181	7.71	–	–	–
		0.133	0.094	0.154	0.170	10.37	–		
10^{-1}	23	0.153	0.112	0.167	0.187	–	–	–	–
		0.143	0.112	0.157	0.171	–	–		
		0.144	0.118	0.156	0.192	–	–		
10^{-0}	23	0.165	0.124	0.172	0.206	–	–	–	–
		0.160	0.123	0.161	0.188	–	–		
		0.164		0.170		–			
10^{-3}	−30	0.226	–	0.206	–	25.61	–	27.21	0.666
		0.238		0.187		25.27		30.38	0.720
		0.246		0.195		23.96		24.90	0.668
		0.239		0.204		25.46			
10^{-3}	−20	0.175	–	0.171	–	19.55	–	21.11	0.628
		0.196		0.162		18.88		29.06	0.720
		0.206		0.168		18.56			
		0.199		0.196		18.78			
10^{-3}	−10	0.157	–	0.158	–	9.54	–	19.35	0.640
		0.171		0.160		11.73		20.30	0.688
		0.172		0.180		13.08		18.81	–
		0.175		0.165		12.24		16.69	0.729
10^{-3}	0	0.153	–	0.160	–	13.15	–	19.27	–
		0.156		0.173		14.13		17.92	0.626
		0.158		0.167		13.81		13.34	0.618
10^{-3}	10	0.126	–	0.157	–	7.18	–	13.30	–
		0.125		0.140		5.94		15.27	–
		0.119		0.145		5.21		13.33	–
								14.19	–
10^{-3}	23	0.116	–	0.142	–	8.68	–	11.54	0.628
		0.113		0.143		8.40		11.75	–
		0.109		0.143		7.76		9.14	0.626
								…	…
10^{-3}	40	0.085	–	0.134	–	5.09	–	6.68	–
		0.086		0.133		4.90		8.36	–
		0.085		0.129		5.50		7.16	–
		0.086		0.139		5.03		…	…
10^{-3}	60	0.054	–	0.109	–	2.33	–	3.92	–
		0.056		0.110		2.06		4.12	–
		0.057		0.109		2.43			
		0.060		0.115		2.36			

References

[1] N. Mills, Polymer foams handbook: engineering and biomechanics applications and design guide, Elsevier Science, 2007, https://doi.org/10.1016/B978-0-7506-8069-1.X5000-4.

[2] P.J. Schuster, Current trends in bumper design for pedestrian impact, SAE Tech, Pap. (2006), https://doi.org/10.4271/2006-01-0464.

[3] L.J. Gibson, M.F. Ashby, Cellular solids: structure and properties, 2nd ed., Cambridge University Press, Cambridge, 1997, https://doi.org/10.1017/CBO9781139878326.

[4] E. Linul, L. Marsavina, Experimental determination of mixed-mode fracture

toughness for rigid polyurethane foams, in: G. Pluvinage, L. Milovic (Eds.), Fracture at all Scales, Springer, Cham, 2017, pp. 221–237, , https://doi.org/10.1007/978-3-319-32634-4_12.
[5] J. Andersons, U. Cābulis, L. Stiebra, M. Kirpļuks, E. Spārniņš, Modeling the mode I fracture toughness of anisotropic low-density rigid PUR and PIR foams, Int. J. Fract. 205 (1) (2017) 111–118, https://doi.org/10.1007/s10704-017-0194-2.
[6] S. Demirel, B.E. Tuna, Evaluation of the cyclic fatigue performance of polyurethane foam in different density and category, Polym. Test. 76 (2019) 146–153, https://doi.org/10.1016/j.polymertesting.2019.03.019.
[7] V.S. Deshpande, N.A. Fleck, Multi-axial yield behaviour of polymer foams, Acta materialia 49 (10) (2001) 1859–1866, https://doi.org/10.1016/S1359-6454(01)00058-1.
[8] A. Reyes, T. Børvik, Quasi-static behaviour of crash components with steel skins and polymer foam cores, Mater. Today Commun. 17 (2018) 541–553, https://doi.org/10.1016/j.mtcomm.2018.09.015.
[9] A. Reyes, T. Børvik, Low velocity impact on crash components with steel skins and polymer foam cores, Int. J. Impact Eng 132 (2019) 103297, , https://doi.org/10.1016/j.ijimpeng.2019.05.011.
[10] A. Krundaeva, G. De Bruyne, F. Gagliardi, W. Van Paepegem, Dynamic compressive strength and crushing properties of expanded polystyrene foam for different strain rates and different temperatures, Polym. Test. 55 (2016) 61–68, https://doi.org/10.1016/j.polymertesting.2016.08.005.
[11] C.R. Siviour, J.L. Jordan, High strain rate mechanics of polymers: a review, J. Dyn, Behav. Mater. 2 (1) (2016) 15–32, https://doi.org/10.1007/s40870-016-0052-8.
[12] J. Zhang, N. Kikuchi, V. Li, A. Yee, G. Nusholtz, Constitutive modeling of polymeric foam material subjected to dynamic crash loading, Int. J. Impact Eng. 21 (5) (1998) 369–386, https://doi.org/10.1016/S0734-743X(97)00087-0.
[13] L. Maheo, S. Guerard, G. Rio, A. Donnard, P. Viot, Multiaxial behavior of foams–experiments and modeling, EPJ Web of Conf. 94 (2015) 04035, https://doi.org/10.1051/epjconf/20159404035.
[14] O. Weißenborn, C. Ebert, M. Gude, Modelling of the strain rate dependent deformation behaviour of rigid polyurethane foams, Polym. Test. 54 (2016) 145–149, https://doi.org/10.1016/j.polymertesting.2016.07.007.
[15] R. Bouix, P. Viot, J.L. Lataillade, Polypropylene foam behaviour under dynamic loadings: Strain rate, density and microstructure effects, Int. J. Impact Eng. 36 (2) (2009) 329–342, https://doi.org/10.1016/j.ijimpeng.2007.11.007.
[16] D.S. Cronin, S. Ouellet, Low density polyethylene, expanded polystyrene and expanded polypropylene: strain rate and size effects on mechanical properties, Polym. Test. 53 (2016) 40–50, https://doi.org/10.1016/j.polymertesting.2016.04.018.
[17] J.L. Halary, F. Laupreˆtre, L. Monnerie, Polymer materials: macroscopic properties and molecular interpretations, John Wiley & Sons, 2011.
[18] S. Arezoo, V.L. Tagarielli, C.R. Siviour, N. Petrinic, Compressive deformation of rohacell foams: effects of strain rate and temperature, Int. J. Impact Eng. 51 (2013) 50–57, https://doi.org/10.1016/j.ijimpeng.2012.07.010.
[19] D.J. Lee, M.K. Kim, J. Walsh, H.K. Jang, H.I. Kim, E.Y. Oh, J. Nam, M. Kim, J. Suhr, Experimental characterization of temperature dependent dynamic properties of glass fiber reinforced polyurethane foams, Polym. Test. 74 (2019) 30–38, https://doi.org/10.1016/j.polymertesting.2018.12.013.
[20] A. Donnard, S. Guerard, L. Maheo, P. Viot, G. Rio, Multiaxial experiments with radial loading paths on a polymeric foam, Polym. Test. 67 (2018) 441–449, https://doi.org/10.1016/j.polymertesting.2018.03.003.
[21] X. Yang, Y. Xia, Q. Zhou, Influence of stress softening on energy-absorption capability of polymeric foams, Mater. Design. 32 (3) (2011) 1167–1176, https://doi.org/10.1016/j.matdes.2010.10.024.
[22] N. Tang, D. Lei, D. Huang, R. Xiao, Mechanical performance of polystyrene foam (EPS): Experimental and numerical analysis, Polym. Test. 73 (2019) 359–365, https://doi.org/10.1016/j.polymertesting.2018.12.001.
[23] K. Senol, A. Shukla, Underwater mechanical behavior of closed cell PVC foams under hydrostatic loading through 3D DIC technique, Polym. Test. 73 (2019) 72–81, https://doi.org/10.1016/j.polymertesting.2018.11.003.
[24] J. Johnsen, F. Grytten, O.S. Hopperstad, A.H. Clausen, Experimental set-up for determination of the large-strain tensile behaviour of polymers at low temperatures, Polym. Test. 53 (2016) 305–313, https://doi.org/10.1016/j.polymertesting.2016.06.011.
[25] H. Akiyama, K. Hirosawa, and H. Kuwabara, Process for producing foamed and molded article of polypropylene resin, April 3 1984. US Patent 4,440,703.
[26] P. Viot, E. Plougonven, D. Bernard, Microtomography on polypropylene foam under dynamic loading: 3D analysis of bead morphology evolution, Compos. Pt. A: Appl. Sci. Manuf. 39 (8) (2008) 1266–1281, https://doi.org/10.1016/j.compositesa.2007.11.014.
[27] L. Andena, F. Caimmi, L. Leonardi, M. Nacucchi, F. De Pascalis, Compression of polystyrene and polypropylene foams for energy absorption applications: A combined mechanical and microstructural study, J. Cell. Plast. 55 (1) (2019) 49–72, https://doi.org/10.1177/0021955X18806794.
[28] E. Fagerholt, eCorr digital image correlation, (2019) (accessed 15 January 2019), http://folk.ntnu.no/egilf/ecorr/doc/.
[29] E. Fagerholt, T. Børvik, O.S. Hopperstad, Measuring discontinuous displacement fields in cracked specimens using digital image correlation with mesh adaptation and crack-path optimization, Opt. Laser. Eng. 51 (3) (2013) 299–310, https://doi.org/10.1016/j.optlaseng.2012.09.010.
[30] F. Pierron, Identification of poisson's ratios of standard and auxetic low-density polymeric foams from full-field measurements, J. Strain Anal. Eng. 45 (4) (2010) 233–253, https://doi.org/10.1243/03093247JSA613.
[31] D. Tripathi, Practical guide to polypropylene, iSmithers Rapra Publishing, 2002.
[32] Y. Kong, J.N. Hay, The measurement of the crystallinity of polymers by DSC, Polym. 43 (14) (2002) 3873–3878, https://doi.org/10.1016/S0032-3861(02)00235-5.
[33] JSP Resins LLC, Arpro® Expanded polypropylene (EPP), (JSP-EPP-STD-0010), 1 2018, Rev. D.
[34] BASF SE, Neopolen® p 9230 k, (30057296/SDS GEN EU/EN), 8 2015, Rev. 4.0.
[35] H. Sasaki, M. Sakaguchi, M. Akiyama, and H. Tokoro, Foamed and expanded beads of polypropylene resin for molding, June 20 2000. US Patent 6,077,875.
[36] M.I. Okereke, C.P. Buckley, C.R. Siviour, Compression of polypropylene across a wide range of strain rates, Mech. Time-Depend. Mater. 16 (4) (2012) 361–379, https://doi.org/10.1007/s11043-012-9167-z.
[37] M. Zrida, H. Laurent, G. Rio, S. Pimbert, V. Grolleau, N. Masmoudi, C. Bradai, Experimental and numerical study of polypropylene behavior using an hyper-visco-hysteresis constitutive law, Comput. Mater. Sci. 45 (2) (2009) 516–527, https://doi.org/10.1016/j.commatsci.2008.11.017.
[38] G. Li, J. Li, J. Wang, J. Feng, Q. Guo, J. Zhou, P. Mitrouchev, The effect of temperature on mechanical properties of polypropylene, in: K. Wang, Y. Wang, J. Strandhagen, T. Yu (Eds.), Adv. Manuf. Autom, Springer, Singapore, 2017, pp. 143–149, , https://doi.org/10.1007/978-981-10-5768-7_14.
[39] B. Alcock, N.O. Cabrera, N.M. Barkoula, C.T. Reynolds, L.E. Govaert, T. Peijs, The effect of temperature and strain rate on the mechanical properties of highly oriented polypropylene tapes and all-polypropylene composites, Compos. Sci. Technol. 67 (10) (2007) 2061–2070, https://doi.org/10.1016/j.compscitech.2006.11.012.
[40] A.D. Drozdov, Effect of temperature on the viscoelastic and viscoplastic behavior of polypropylene, Mech. Time-Depend. Mater. 14 (4) (2010) 411–434, https://doi.org/10.1007/s11043-010-9118-5.